Society For Biomaterials

# Cell-adhesive thermogelling PNIPAAm/hyaluronic acid cell delivery hydrogels for potential application as minimally invasive retinal therapeutics

**M. A. Jafar Mazumder,[1*] Scott D. Fitzpatrick,[2*] Ben Muirhead,[2] Heather Sheardown[1,2]**

[1]Department of Chemical Engineering, McMaster University, 1280 Main St. West, Hamilton, Ontario, Canada L8S 4L7
[2]School of Biomedical Engineering, McMaster University, 1280 Main St. West, Hamilton, Ontario, Canada L8S 4L7

Received 11 September 2011; revised 28 October 2011; accepted 7 November 2011
Published online 10 April 2012 in Wiley Online Library (wileyonlinelibrary.com). DOI: 10.1002/jbm.a.34021

**Abstract:** Copolymers of *N*-isopropylacrylamide (NIPAAm) and acrylic acid *N*-hydroxysuccinimide (NAS) were synthesized via free radical polymerization and conjugated with amine-functionalized hyaluronic acid (HA) and cell adhesive RGDS peptides. These novel copolymers were designed to facilitate noninvasive delivery of a liquid suspension of cells into the delicate subretinal space for treatment of retinal degenerative diseases such as age-related macular degeneration (AMD) and diabetic retinopathy. The various synthesized copolymers all displayed subphysiological phase transition temperatures, thereby allowing temperature-induced scaffold formation and subsequent entrapment of transplanted cells within an adhesive support matrix. Successful grafting of HA and RGDS peptides were confirmed with Fourier Transform Infrared (FTIR) spectroscopy and quantified with $^1$H Nuclear Magnetic Resonance (NMR) spectroscopy. All copolymers demonstrated excellent compatibility with retinal pigment epithelial (RPE) cells in culture and minimal host response was observed following subcutaneous implantation into hairless SKH1-E mice (strain code 447). © 2012 Wiley Periodicals, Inc. J Biomed Mater Res Part A: 100A: 1877–1887, 2012.

**Key Words:** thermally responsive, retina, cell delivery, poly(*N*-isopropylacrylamide), hyaluronic acid

**How to cite this article:** Jafar Mazumder MA, Fitzpatrick SD, Muirhead B, Sheardown H. 2012. Cell-adhesive thermogelling PNIPAAm/hyaluronic acid cell delivery hydrogels for potential application as minimally invasive retinal therapeutics. J Biomed Mater Res Part A 2012:100A:1877–1887.

## INTRODUCTION

Cell-based therapies and in particular stem cell technology have undergone numerous exciting advances in recent years that may have profound implications in the development of novel retinal treatments. Takahashi and Yamanaka recently developed a method to genetically reprogram differentiated fibroblast cells into a pluripotent, embryonic stem cell-like state through the introduction of four factors; Oct3/4, Sox2, c-Myc, and Klf4.[1] It is now possible to produce induced pluripotent stem (iPS) cells from adult somatic tissues to generate autologous cell populations of nearly all tissues in the body, including the eye.[2] In 2006, MacLaren et al. demonstrated that it may one day be possible to repopulate damaged or diseased retinas with healthy, functioning photoreceptor cells.[3] West et al. developed a method to improve integration of photoreceptor precursor cells into the outer nuclear layer (ONL) through temporary disruption of the outer limiting membrane (OLM) using a glial toxin, alpha-amino adipic acid (AAA).[4] In a recent breakthrough, Eiraku et al. demonstrated the ability to generate complex retinal tissue through self-organizing optic-cup morphogenesis in a three dimensional culture setting.[5] However, while photoreceptor cell therapy is an exciting strategy with tremendous therapeutic potential, proper integration and organized wiring with the neural retinal circuitry may represent an extremely difficult process to overcome, especially following retrograde degeneration.[6] Therefore, while it is crucial to continue to investigate photoreceptor regeneration strategies, clinical application remains a distant prospect.[7] It is likely that success in the treatment of retinal degenerative diseases such as age-related macular degeneration (AMD), will stem from early-stage preventative measures aimed at preserving retinal health through modulation of the subretinal microenvironment.[2] Early-stage delivery of protective cells, such as retinal pigment epithelial (RPE) cells, may provide a means of maintaining retinal homeostasis and preventing the onset of photoreceptor degeneration and loss of vision. The retinal pigment epithelium is a monolayer of metabolically active cells that exists between the photoreceptors and the underlying vasculature, the choriocapillaries.[2] The RPE express several neurotrophic factors such as platelet-derived growth factor (PDGF), pigment-derived

*These authors contributed equally to this work.
**Correspondence to:** H. Sheardown; e-mail: sheardow@mcmaster.ca
Contract grant sponsors: NSERC, 20/20 NSERC Ophthalmic Materials Network

epithelial factor (PDEF), vascular endothelial growth factor (VEGF), and epidermal growth factor (EGF), which help maintain photoreceptor health.[8] Furthermore, the RPE is crucial for visual health as it provides nourishment for the photoreceptors, forms the outer component of the blood-retinal barrier (BRB) and clears the subretinal space of debris through phagocytosis of photoreceptor outer segments.[9] In many retinal degenerative diseases, such as AMD, progressive dysfunction of the RPE leads to secondary deterioration of photoreceptor health and visual function.[2] It has long been known that restoration of RPE health through cell therapy may prevent the subsequent loss of photoreceptors; RPE isolation and transplantation was first attempted over 25 years ago.[10,11]

However, delivery of cells into the highly complex, delicate subretinal space represents a significant challenge. In previous studies, cells were delivered into the subretinal space via syringe as a bolus injection.[12] While this method is considered minimally invasive, it is relatively ineffective, as bolus injections tend to offer little in the way of sustained guidance cues or substrates for cellular adhesion.[13] As a result, there is poor control over transplanted cell fate, uncontrolled leakage from the injection site, aggregation of nonfunctional cell islands, poor integration into host tissues, and cell death.[12–14] Bolus cell injections likely result in failure of the cells to adhere efficiently to the native basement membrane in the subretinal space, the Bruch's membrane, due to age or disease-related structural changes in the collagenous membrane.[15] There have been numerous attempts to increase the capacity of the aged Bruch's membrane to support the growth and differentiation of transplanted cells; however, success has thus far been limited.[16,17] RPE cells are anchorage-dependent and therefore it is crucial to provide the transplanted cells with an adequate support matrix whether it is the native Bruch's membrane, or a synthetic extracellular matrix analog.[12] In the absence of an appropriate adhesion substrate, such as in the case of an aged Bruch's membrane, RPEs undergo a process of adhesion-dependent apoptosis, or anoikis.[12] Consequently, an alternative delivery approach is to seed and expand cells *ex vivo* on or within a biomaterial scaffold and to implant the construct directly into the subretinal space.[2] While delivering cells within a scaffold addresses many of the shortcomings of bolus injections by providing a substrate for adhesion, isolating cells to the target tissues and offering a scaffold from which guidance molecules may be released for sustained periods, implantation of a solid construct into the delicate subretinal space is inherently more invasive than simple injections. As it is highly likely that the ultimate success of retinal cell therapy will require minimally invasive delivery techniques, in this work, we have synthesized thermoresponsive cell adhesive biomaterial scaffolds that combine the minimally invasive delivery of bolus injections with the advantages of a solid extracellular support matrix.

Poly (*N*-isopropylacrylamide) (PNIPAAm), a synthetic polymer that exists as a liquid at room temperature but rapidly gels when heated above a lower critical solution temperature (LCST) around 32°C, forms the major component of the biomaterial scaffold, allowing noninvasive delivery via syringe and subsequent scaffold formation *in situ* following temperature-induced gelation. In our previous work,[18] linear chains of amine-terminated PNIPAAm were grafted along the backbone of type I bovine collagen to provide a cell-adhesive, thermogelling copolymer to serve as a vehicle for subretinal cell delivery. In this work, cellular adhesive properties were introduced into the scaffolds by replacing the large, bulky collagenous backbone with a small cell adhesion peptide sequence, arginine–glycine–aspartic acid–serine (RGDS), which serves as the major binding sequence of extracellular matrix proteins fibronectin, laminin, and collagen, and appears to dictate the adhesion of RPE cells to the Bruch's membrane.[19] In addition, hyaluronic acid (HA), which is a lubricating polysaccharide that has been shown to improve cellular adhesion, proliferation and migration,[20] was incorporated into the final copolymers to enhance the ability of the scaffolds to act as cellular substrates. The synthesis and characterization of thermoresponsive, cell adhesive PNIPAAm/HA-based copolymers designed for subretinal transplantation of anchorage-dependent RPE cells is described herein.

## MATERIALS AND METHODS

Acrylic acid *N*-hydroxysuccinimide (NAS), benzoyl peroxide (97%), adipic acid dihydrazide (≥98%) (ADH), 1-hydroxybenzotriazole hydrate (97%) (HOBT), and 1-ethyl-3-(3-dimethylaminopropyl)-carbodiimide hydrochloride (EDC) were purchased from Sigma-Aldrich (Oakville, ON, Canada), and used as received. Hyaluronic acid (HA) (169 kDa) was purchased from Lifecore Biomedical (Chaska, MN) and used as received. *N*-isopropylacrylamide (NIPAAm) (97%) was purchased from Sigma- Aldrich (Oakville, ON, Canada), and was purified by recrystallization from a toluene/hexane mixture. RGDS (433.4 Da) was purchased from American Peptide (Sunnyvale, CA), and was used as received. 1,4 dioxane, toluene, hexane, tetrahydrofuran (THF), dimethylsulfoxide (DMSO), and anhydrous ethyl ether were purchased from Caledon Laboratories (Caledon, ON), and were used as received. Sodium hydroxide and hydrochloric acid solutions were purchased as concentrates from Anachemia Chemical (Rouses Point, NY), and were prepared by diluting to 1.0 or 0.1*M* with deionized water. Deionized water with a resistivity of 18.2 MΩ cm was prepared using a Milli-pore Barnstead water purification system (Graham, NC). Phosphate buffered saline solution (PBS, pH 7.4) was purchased from McMaster University Health Science facilities and used as received. Cellulose dialysis membranes with molecular weight cutoff values of 1–12 kg/mol were purchased from Spectrum Laboratories Inc (Rancho Dominguez, CA). Human RPE cells (CRL-2502) were purchased commercially from ATCC (Manassas, VA) and were cultured under $CO_2$ (37°C, 5% $CO_2$, 95% air, 100% humidity). DMEM-F12 culture medium (Gibco, Carlsbad, CA) was supplemented with FBS (6.25% final concentration, Gibco), 1 × glutamate (1% final concentration, Gibco), penicillin–streptomycin (1% final concentration, Gibco), and sodium bicarbonate (0.8% final

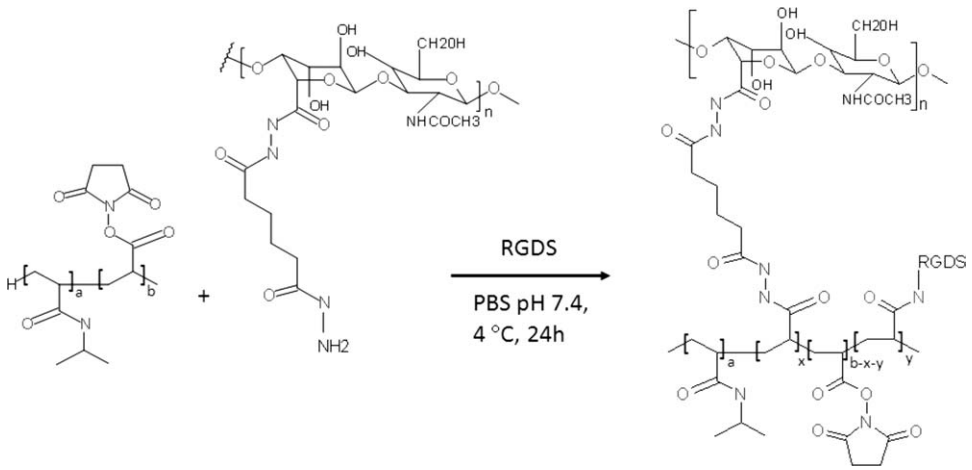


**SCHEME 1.** Reaction scheme detailing the grafting of amine-functionalized hyaluronic acid and cell-adhesive RGDS peptide sequences along the p(NIPAAm-*co*-NAS) copolymer backbone.

concentration, Gibco). Trypan Blue (0.4%) was purchased from Gibco and used as received.

### Synthesis of p(NIPAAm-co-NAS)

p(NIPAAm-*co*-NAS) (PNN) copolymers were synthesized by free radical polymerization. NIPAAm (4.298 g, 37.89 mmol), NAS (0.7181 g, 4.21 mmol), and BPO (0.102 g, 0.42 mmol, 1 mol % relative to monomer) were dissolved in 45 mL 1,4 dioxane to form a 10 wt % monomer solution (90: 10 feed ratio of NIPAAm: NAS). Dry nitrogen was bubbled through the solution for 15 min. The reaction vessel was then sealed and heated to 70°C for 24 h in a temperature controlled oil bath with continuous stirring to provide uniform mixing. The polymer solution was then cooled to room temperature and isolated by precipitation in anhydrous ethyl ether (1 L). The precipitated polymer was dried in a vacuum oven at 50°C for 48 h. The copolymer, p(NIPAAm-*co*-NAS) (90:10) (PNN-10), was purified twice by precipitation from THF into anhydrous ethyl ether and then dried to a constant weight in a vacuum oven at 50°C. Copolymer yield for PNN-10 was found to be 86% (4.3 g). PNN-10 was further purified for *in vitro* and *in vivo* studies by extensive dialysis (3.5 kg/mol MW cut-off) against deionized water at 4°C. The dialyzed product was freeze-dried, and stored at −20°C.

Polymerization and purification of a 95:5 NIPAAm: NAS copolymer (PNN-5) was also performed using similar methods as described. Briefly, NIPAAm (4.639 g, 40.96 mmol), NAS (0.3652 g, 2.156 mmol), and BPO (0.1046 g, 0.431 mmol) were dissolved in 45 mL 1,4 dioxane, and polymerization was carried out for 24 h at 70°C. The copolymer was isolated through precipitation in anhydrous ethyl ether and purified twice from THF. The PNN-5 copolymer was dried to constant weight in a vacuum oven at 50°C and the yield was found to be 91% (4.55 g).

### Preparation of amine-functionalized hyaluronic acid

Amine-functionalized hyaluronic acid was prepared as described previously in the literature.[21] Briefly, HA (169 kDa) (250 mg, 0.625 mmol, based on the repeating unit MW) was dissolved in 47 mL of deionized water. ADH (5.5 g, 31.57 mmol) was added under continuous stirring. EDC (0.6 g, 3.12 mmol) and HOBT (0.478 g, 3.12 mmol) were dissolved in a 2.5 mL solution of DMSO and $H_2O$ (1:1), and then added to the polymer solution under stirring. The pH was adjusted to 4.8 by adding 0.1*M* HCl, and the reaction was continued under gentle stirring at room temperature (20°C) for 20 h in an oil bath. HA-ADH was purified by extensive dialysis (3.5 kg/mol MW cut-off) with deionized water at 4°C. The purified amine-functionalized HA was then lyophilized, and stored at −20°C. The final amine content was determined by $^1$H Nuclear Magnetic Resonance (NMR), and found to be 24 mol % of the total carboxylic unit for HA.

### Preparation of HA grafted PNIPAAm

PNN-10 (0.593 g, 0.502 mmol NAS) was dissolved in 20 mL deionized water. HA-ADH (0.08 g, 0.201 mmol, based on repeating unit MW of HA) was dissolved in 10 mL deionized water, and added to the polymer solution under stirring. The reaction mixture was stirred for 24 h at room temperature (20°C). The HA grafted copolymer, p(NIPAAm-*co*-NAS-HA) (PNN-HA) was dialyzed in deionized water (50 kg/mol MW cut-off). The resulting polymer solution was freeze-dried, and stored at −20°C.

### Preparation of RGDS grafted PNIPAAm

PNN-10 (0.7506 g, 0.636 mmol NAS) was dissolved in 10 mL PBS (pH 7.4) in a 20 mL glass vial. RGDS (110 mg, 0.253 mmol) was dissolved in 5 mL PBS (pH 7.4), and added to the polymer solution. The reaction was allowed to proceed for 24 h at 4°C. The RGDS-grafted copolymer, p(NIPAAm-*co*-NAS-RGDS) (PNN-RGDS), was extensively dialyzed in deionized water (3.5 kg/mol MW cut-off) at 4°C. The resulting polymer solution was freeze-dried, and stored at −20°C.

### Preparation of HA and RGDS grafted PNIPAAm

PNN-10 (0.75 g, 0.636 mmol NAS) was dissolved in 10 mL PBS (pH 7.4) in a 20 mL glass vial. RGDS (50 mg, 0.115 mmol) and HA-ADH (100.8 mg, 0.254 mmol based on

repeating unit MW of HA) were separately dissolved in 5 mL PBS (pH 7.4) and added to the polymer solution, Scheme 1. The reaction was allowed to proceed for 24 h at 4°C under stirring. The HA and RGDS grafted copolymer p(NIPAAm-*co*-NAS-HA.RGDS) (PNN-HA.RGDS) was extensively dialyzed in deionized water (50 kg/mol MW cut-off) at 4°C. The resulting polymer solution was freeze-dried, and stored at −20°C.

**Material characterization**

The structure of the various PNN-5 and PNN-10 copolymers was characterized by Thermo Fisher Nicolet 6700 FTIR spectrometer. Copolymer composition was determined by $^1$H-NMR spectroscopy using a Bruker AV 200 spectrometer with DMSO-$d_6$ as a solvent. The degree of labeling with HA and RGDS was determined by $^1$H-NMR spectroscopy using a Bruker 600 spectrometer with $D_2O$ as a solvent.

**Molecular weight determination**

A Ubbelohde viscometer (viscometer constant: 0.00314 cSt/s), was used to determine the MW of p(NIPAAm-*co*-NAS) dissolved in methanol at 25.0 ± 0.1°C. Prior to measurement, all stock solutions were filtered through a 0.20 μm membrane filter. The intrinsic viscosity [η] was calculated by extrapolation of the Huggins plot ($\eta_{sp}/c$ versus c) to a concentration of zero. The polymer MW was calculated from the intrinsic viscosity using the relationship $[\eta] = KM^a$ with values for $K$ and $a$ found in the literature.[22]

**Characterization of lower critical solution temperature**

The lower critical solution temperatures (LCST) of the hydrogel copolymer solutions were measured by differential scanning calorimetry (DSC, TA Instruments 2910) and UV/vis spectrophotometry (Cary 300). To determine the thermal transition temperature by DSC, samples (15% w/v in PBS) were heated in hermetic pans from 0 to 70°C at a heating rate of 2°C/min. The temperature at the maximum endothermal peak in the DSC curve was considered as the thermal transition temperature. Transmittance measurements as a function of temperature were assessed to verify LCST values obtained via DSC. Polymer samples were dissolved in PBS (2.5% w/v) and placed in 4-mL UV cuvettes. The samples were heated from 25 to 45°C at a rate of 1°C/min and transmittance measurements were recorded every 30 s.

**Copolymer morphology**

High-resolution images of the internal pore structure of the various hydrogels were obtained using a Phillips 515 scanning electron microscope (SEM). Polymer samples were swelled (25% w/v) in PBS (pH 7.4) at 37°C for 2 days. Excess PBS was then removed and the samples were cryo-preserved by immersion in a liquid nitrogen bath. The copolymers were then lyophilized and the dried samples were mechanically fractured to expose the internal structure. A 10 nm platinum coating was applied using a Precision Etching Coating System (Model 682) to increase sample conductance and allow surface visualization. Images were captured with Mektech URSA 100 Rev. 1.30 imaging software.

**Water content**

The water content of the hydrogel was measured gravimetrically. An aqueous copolymer solution (15% w/v) was placed in a preweighed polystyrene Petri dish. The covered dish was then placed into an incubator at 37°C for 6 h. The supernatant was then removed and the hydrogel pellet was gently dabbed dry with tissue paper to remove residual surface water. The Petri dish was weighed to determine the wet weight of the hydrogel, and then both the wet hydrogel and supernatant were dried to constant weight by heating at 65°C. The water content was calculated using the following equation:

$$\text{Water Content} = \frac{(m_w - m_d)}{m_d} \times 100\%$$

where $m_w$ is the weight of the wet hydrogel and $m_d$ is the weight of the dry hydrogel.

**Cell culture**

To remove biological contaminants, polymer samples were dialyzed extensively in deionized water (3.5 kg/mol MW cut-off), freeze dried and pretreated with a solution of PBS and penicillin-streptomycin (3:1 v/v). RPE cells were seeded at a density of 10,000 cells per well in a 48-well tissue culture treated polystyrene (TCPS) plate. Cells were incubated in serum supplemented DMEM-F12 culture medium for 2 h to allow adhesion to the culture dish. Cell supernatant was then aspirated and replaced with fresh medium containing 10 mg of PNN-10, PNN-HA, PNN-RGDS, or PNN-HA.RGDS. Fresh DMEM-F12 culture medium containing no polymer was used as a control. The samples were placed in the incubator and after 96 h, the culture medium was aspirated and viability was assessed using a Trypan Blue exclusion assay (0.4%, Gibco). Live and dead cells were counted using a hemocytometer.

**Subcutaneous injections**

Protocols prepared by the McMaster University Animal Research Ethics Board for the care and use of laboratory animals have been observed. Dry polymer samples were sterilized with ethylene oxide (EO) gas, which has been shown to be a minimally reactive and effective method of sterilizing biomaterials.[23] EO sterilization was carried out at the McMaster University histopathology laboratory and was achieved in a 100% ethylene oxide atmosphere at 57°C for 2 h. Samples were then exposed to sterile air for 15 h to remove residual EO. The samples were then dissolved in 10 mL aliquots of Fischer Brand medical grade saline to form 15% w/v solutions. Prior to injection, mice were anaesthetized with isofluorane gas. The polymer samples, syringes and injection site were precooled to prevent premature gelation of the polymer within the syringe. Polymer suspensions (150 μL) were injected subcutaneously between the shoulder blades of hairless SKH1-E mice (strain code 447). Mice were sacrificed at 3, 7, 20, and 40 days ($n$ = 1, 3, 2, and 2, respectively). The polymer and surrounding tissues were excised, fixed in a 4% neutral

buffered formalin solution for 24 h, and embedded in paraffin wax. Processed tissue was then sectioned into 4-μm slices using a Leica RM2255 microtome. Sections were stained with hematoxylin and eosin (H&E), and images were collected using an Olympus BX51 optical microscope with QImaging Retiga 2000R camera and Image-Pro Plus (version 7.0) software. The liver and spleen of mice at day 40 were removed, weighed, processed for histological analysis as described above and compared with a control, which received no injection.

### Statistical analysis

A one-factor analysis of variance (ANOVA) was used to analyze scaffold water content and the effect of scaffold presence on RPE viability using $\alpha = 0.05$. A *post-hoc* analysis was performed on scaffold water content using Tukey's HSD test. Statistical analysis of mean viability and scaffold water content was performed using PASW Statistics 18 (SPSS, IL). All error bars represent standard deviations.

## RESULTS AND DISCUSSIONS

### Synthesis and characterization of p(NIPAAm-*co*-NAS) copolymer

Copolymers with varying ratios of NIPAAm and NAS were prepared by free-radical polymerization. NAS was selected as the reactive comonomer to provide facile conjugation with biological molecules, such as cell adhesion peptides, without the need for harsh chemical conditions.[24] Additionally, NAS polymerizes efficiently with a wide range of (meth)acrylate[25] and (meth)acrylamide[26] monomers and is commercially available. In our previous work,[18] we examined the potential use of type 1 collagen with linear chains of amine-terminated PNIPAAm grafted along its backbone as a cell delivery scaffold. Collagen was selected as it is one of the major components of the Bruch's membrane and could therefore mimic the natural RPE basement membrane. However, its large size, and limited solubility made it difficult to obtain reproducible polymers. In this work, the bulky collagen backbone has been replaced with small RGDS cell binding peptides, which Tezel et al. suggest may be the most important adhesion sequence that dictates long-term support and survival of RPE cells.[19] The RGD peptide is a bioactive sequence capable of binding surface integrins on RPE cells and has been shown to influence cellular adhesion, migration, proliferation, and differentiation.[27] The p(NIPAAm-*co*-NAS)-based scaffolds have been conjugated with an RGDS sequence to create thermoresponsive cell delivery vehicles that mimic the native Bruch's membrane. Replacing the bulky collagen molecule with small RGDS peptides eliminates superfluous protein structures, allowing for a more compact polymer scaffold without compromising the potential for cellular adhesion. Less volume would therefore be required for delivery into the limited subretinal space. Furthermore, we hypothesized that the incorporation of hyaluronic acid (HA), or hyaluronan, would improve the performance of the p(NIPAAm-*co*-NAS) copolymers as support matrices for transplanted RPE cells. HA is a naturally occurring hydrophilic lubricating polysaccharide composed of repeating units of *N*-acetyl-D-glucosamine and D-glucuronic acid.[20] It is biocompatible, enzymatically degradable and is found in the vitreous humor, synovial fluid, umbilical cord, and the ECM of most tissues.[28,29] In the eye, HA has demonstrated promising results in the treatment of dry eye,[30,31] has been shown to promote corneal wound healing[32] and is used for visco-supplementation in cataract surgery.[33] The Sheardown group has demonstrated that HA can decrease protein uptake and improve wettability in silicone hydrogel contact lenses.[34] HA has also been shown to have a number of cellular functions, including attachment, migration and proliferation.[20] Thus, amine-functionalized HA was incorporated into the copolymers via coupling with NAS.

There are a number of manuscripts that report the synthesis of poly(NIPAAm-*co*-NAS) copolymers, with a specific interest in protein-reactive systems.[24,35] Similarly, there are a number of NIPAAm-HA materials in the literature.[36,37] However, the majority of these materials attach HA to end-functionalized NIPAAm, whereas our system yields distribution of HA throughout, which we believe will be beneficial for providing a synthetic extracellular matrix. Furthermore, our system allows a high degree of flexibility over the molecular weight of HA incorporated and the copolymer content of HA and RGDS. To our knowledge, there are no other reports of NAS chemistry used to functionalize NIPAAm-based copolymers with hyaluronic acid. Several groups have successfully utilized NAS chemistry to graft cell adhesive RGDS peptides onto NIPAAm-based copolymers to create bioactive scaffolds. For instance, Smith et al. demonstrated the ability to generate cell adhesive NIPAAm-based copolymers through RGD conjugation with protein-reactive NAS groups[38] and later used similar copolymers to facilitate the attachment of bone-morphogenetic protein-responsive C1C12 cells.[39] Li et al. reported the ability to recruit multiple cell lines into artificial corneal implants comprised of copolymers of NIPAAm, NAS, acrylic acid, and RGD[40]. Finally, Quan et al. developed an elegant system for tumor-triggered drug release utilizing NAS chemistry to conjugate protected RGD groups onto NIPAAm-based copolymers, which were then coupled with cyclodextrin to create self-assembled, noncovalently coupled micelles (NCCM).[41] The design employed the subtle physiological changes in the surrounding tumor tissues (pH = 6.8, $T > 37^{\circ}$C) to deprotect the RGD group allowing targeting of tumor cells, which overexpress receptors for RGD, and intracellular destabilization of the NCCM and targeted release.[41] To our knowledge, these are the only examples of copolymers containing NIPAAm, NAS, and RGD. We were unable to find evidence of HA-containing RGDS-grafted NIPAAm copolymers in the literature.

FTIR was used to confirm the final structure of the p(NIPAAm-*co*-NAS) copolymer, Figure 1. The FTIR spectrum shows that the NIPAAm and NAS monomers [Fig. 1(a,b)] have strong characteristic peaks at 1622 and 1408 $cm^{-1}$, which are attributed to C=C and $CH_2$= stretching vibration, respectively. However, these two peaks disappear after successful synthesis of the PNN-10 copolymer, Figure 1(c). The NIPAAm spectrum contains characteristic peaks of C=O and N—H stretching of amide groups I and II around 1652 and

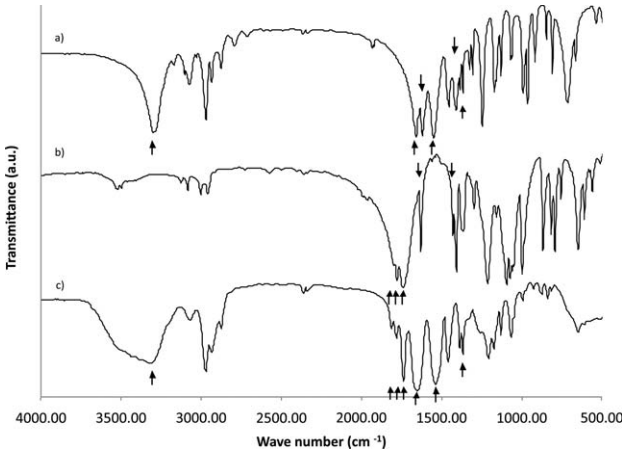


**FIGURE 1.** FTIR spectra of (a) NIPAAm, (b) NAS, and (c) PNN-10 copolymer. FTIR was used to confirm the successful copolymerization of poly(NIPAAm-*co*-NAS).

1540 $cm^{-1}$ respectively. Moreover, stretching vibration of the N—H amine group appears around 3309 $cm^{-1}$, and vibration of the isopropyl group around 1380 $cm^{-1}$ was also observed. The characteristic succinimide peaks around 1812, 1781, and 1735 $cm^{-1}$ for NAS monomer were observed. The PNN-10 spectra contain succinimide absorption peaks as well as peaks at 3317 and 1660 $cm^{-1}$, corresponding to the NIPAAm groups mentioned above, confirming the final structure of the PNN-10 copolymer.

The $^1$H-NMR spectra in Figure 2 confirms successful copolymerization of PNN-10 and grafting of HA and RGDS onto the copolymer backbone. In the PNN-10 spectrum, characteristic succinimide $CH_2$ peaks are observed at 2.9 ppm and the CH peak associated with the isopropyl group

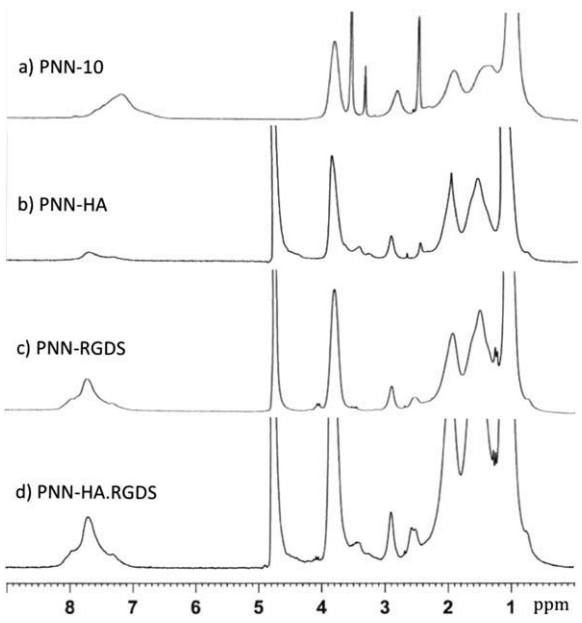


**FIGURE 2.** $^1$H-NMR spectra of (a) PNN-10, (b) PNN-HA, (c) PNN-RGDS, and (d) PNN-HA.RGDS. $^1$H-NMR was used to confirm the successful grafting of HA and RGDS onto the PNN-10 copolymer backbone and to quantify grafting efficiency.

**TABLE 1. Polymer Feed Ratios, Final Copolymer Composition, Molecular Weight Determined via Ubbelohde Viscometer, and Phase Transition Temperatures Determined with DSC**

| Polymer (Feed Ratio) | Composition[a] | MW (kg/mol)[b] | LCST[c] |
|---|---|---|---|
| p(NIPAAm-*co*-NAS) (95:5) | 94:5 (±1) | 43 | 29 |
| p(NIPAAM-*co*-NAS) (90:10) | 90:10 (±2) | 30 | 27 |
| p(NIPAAM-*co*-NAS-HA) | 90:6:4 | | 31 |
| p(NIPAAM-*co*-NAS-RGDS) | 90:6:4 | | 31 |
| p(NIPAAM-*co*-NAS-HA.RGDS) | 90:4:4:2 | | 32 |

[a] Copolymer composition in mol % determined by $^1$H-NMR.
[b] $M_w$ obtained from viscometry data.
[c] LCST obtained from differential scanning calorimetry.

of NIPAAm is observed at 3.9 ppm. In the PNN-HA spectrum, the HA ring appears broadly in the range of 3–4 ppm and a $CH_2$ peak from the ADH linker is observed at 2.4 ppm. RGDS peaks are observed at 2.5 and 4 ppm in the PNN-RGDS spectrum. Finally, in the PNN-HA.RGDS spectrum, the $CH_2$ peak of the ADH linker is observed around 2.4–2.5 ppm alongside RGDS and a distinct RGDS peak appears at 4 ppm. Additionally, the broad peak associated with the HA ring is observed between 3 and 4 ppm, thus confirming the facile conjugation with biological molecules in the absence of harsh chemical conditions through NAS functionality. The composition of the synthesized copolymers and grafting density of all modified polymers were calculated with $^1$H-NMR. Monomer feed ratios and copolymer compositions are listed in Table I. Copolymer compositions were found to be consistent with the feed ratios.

### LCST of the copolymers

Both DSC and UV spectrophotometry confirmed subphysiological phase transition temperatures for the various scaffolds, as shown in Table I and Figure 3, respectively. Subphysiological phase transition temperatures are critical for the application of cell or drug delivery scaffolds that are designed to utilize body temperature to stimulate *in situ* gel formation. Polymerization with hydrophobic co-monomers such as dimethyl-γ-butyrolactone acrylate (DBA)[42] lowers

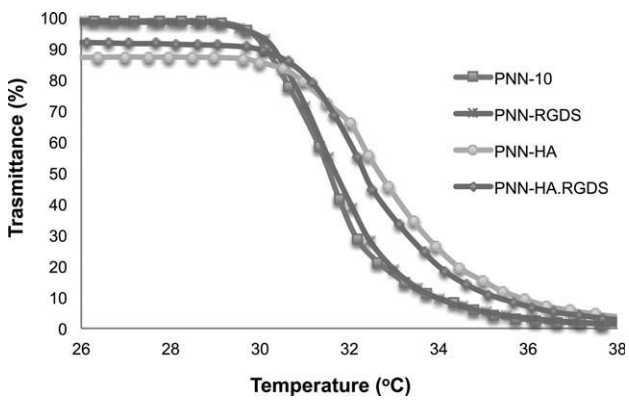


**FIGURE 3.** UV spectrophotometry was used to confirm LCST values obtained via DSC. Rapid gelling kinetics are observed by the sudden decrease in transmittance as the cloud point is reached.

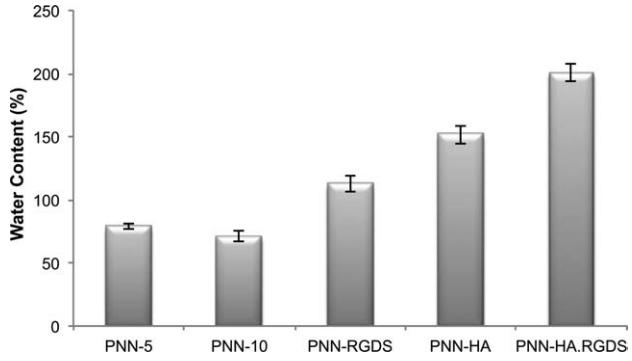


**FIGURE 4.** Water content of the various copolymers. Incorporation of HA and RGDS increased copolymer water content, whereas hydrophobic NAS resulted in a decrease. The difference among mean water content for each sample was statistically significant ($p < 0.001$) except between PNN-5 and PNN-10 ($p = 0.499$).

the LCST, whereas addition of hydrophilic comonomers such as acrylic acid[24] results in an increase. Therefore copolymerization with NAS in a 95:5 molar feed ratio of NIPAAm: NAS, produced a copolymer with an LCST of 29°C, slightly lower than unmodified PNIPAAm, which is typically reported as 32°C.[18] Increasing the NAS content of the p(NIPAAm-*co*-NAS) copolymer to 10 mol % further decreased the LCST to 27°C, whereas incorporation of either HA or RGDS into PNN-10 increased the LCST to 31°C. Incorporation of both HA and RGDS into PNN-10 further increased the LCST to 32°C.

From the transmittance curves obtained via UV spectrophotometry, rapid gelation kinetics can be observed by the sudden decrease in transmittance when samples are heated above their LCST. Rapid gelation is imperative to induce cellular entrapment at the injection site and prevent the efflux of cells away from target tissues and into the vitreous cavity. The presence of small amounts of bulky polysaccharide HA appears to slightly delay gelling kinetics as copolymers lacking HA displayed a sharper decrease in transmittance. The small HA content likely impedes the self-assembly of PNIPAAm and NAS groups to some extent. However, gelation kinetics remain sufficiently rapid for cell delivery purposes as scaffold formation was observed almost instantaneously upon injection into heated aqueous medium and upon subcutaneous injection into mice. Furthermore, it may be possible to incorporate lower molecular weight HA, which will minimize this problem.

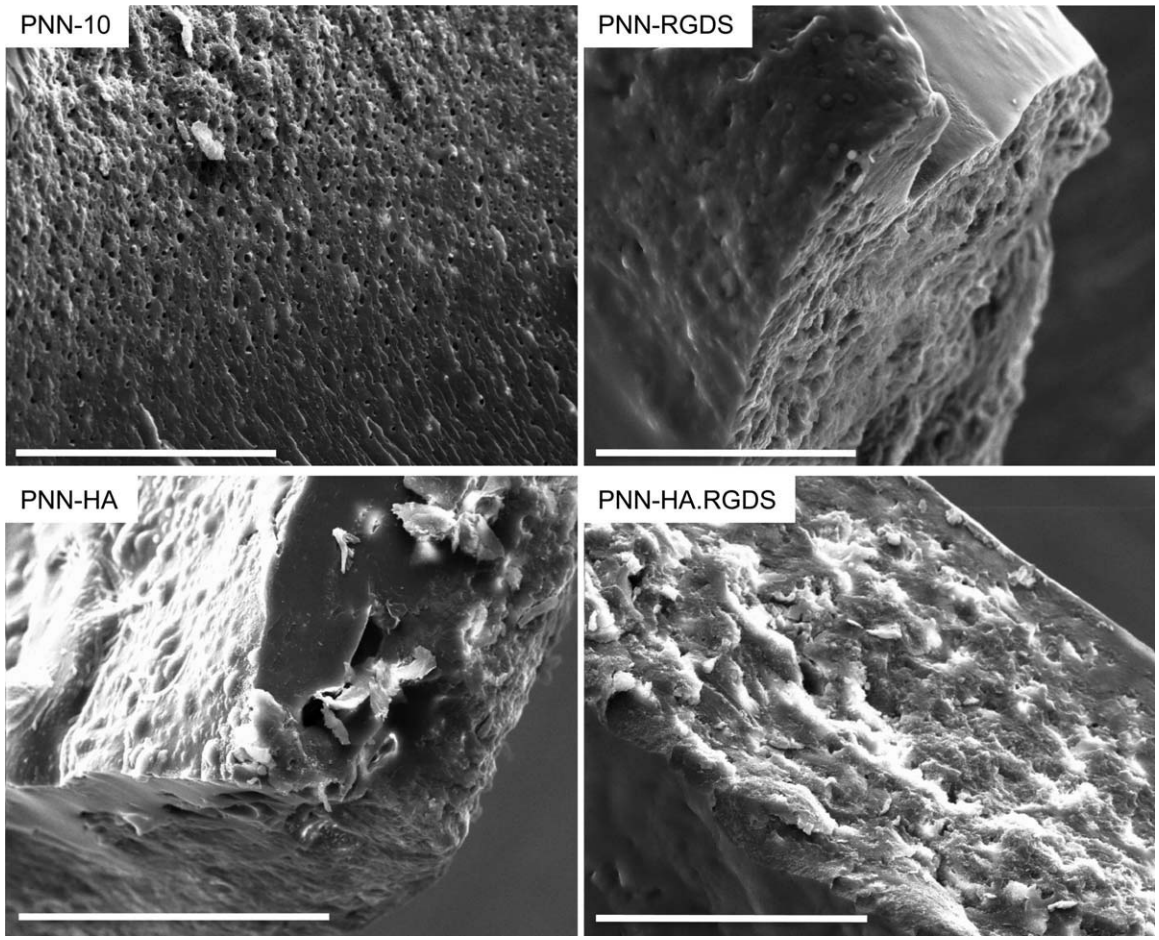


**FIGURE 5.** SEM images of the internal pore structure of the various copolymers. Dried polymers were mechanically fractured to expose the internal structure. The internal copolymer pore structure appears to become increasingly amorphous as a function of increasing water content. Scale bar = 100 μm.

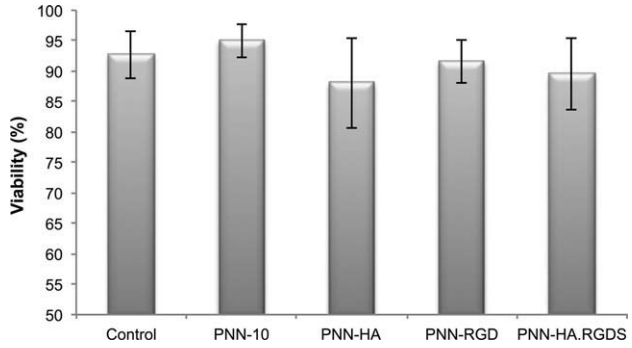


**FIGURE 6.** Retinal pigment epithelial cells demonstrated excellent compatibility with the various copolymers in culture. RPE cells seeded on a tissue culture-treated polystyrene plate served as a control. Viability remained high in all conditions and there was no statistically significant difference among the means ($p = 0.103$).

### Water content

The water content of the various copolymers was consistent with the LCST findings. Increasing the NAS content from 5 to 10 mol % in the PNN copolymer increased the hydrophobic nature of the material, which decreased the LCST and appears to have slightly decreased the overall water content. The incorporation of HA and RGDS in PNN-HA and PNN-RGDS, which effectively increased copolymer LCST, also yielded copolymers with a higher water content. Finally, PNN-HA.RGDS, which had the highest LCST at 32°C, also had the highest observed water content, Figure 4.

### Structural properties of the hydrogels

High-resolution images of the microstructure of the various polymers were obtained using SEM, as shown in Figure 5. From the SEM micrographs, it appears that copolymer morphology and surface roughness correspond closely with water content. As copolymer water content increases, the internal pore morphology appears to become increasingly amorphous and the surface roughness increases. PNN-10, which was the most hydrophobic of the copolymers tested (PNN-5 was not examined) and had the lowest water content, possessed a relatively defined, closed-pore structure. Whereas, PNN-HA.RGDS, which was the most hydrophilic copolymer with the highest water content, had a much more amorphous, interconnected internal pore morphology. The differences in internal pore morphology likely arise during copolymer gelation as the more hydrophobic copolymer tends to collapse more tightly in on itself to minimize interfacial tension at the polymer–aqueous boundary layer. As a result, the hydrophobic copolymer tends to form closed, spherical pockets surrounding aqueous domains within the hydrogel. As copolymer hydrophilicity increases, interfacial tension decreases, leading to greater interconnectivity between the pores. This behavior explains the relatively smooth exterior shell of PNN-10 and the rough surface possessed by PNN-HA.RGDS (Supporting Information Fig.). Copolymers with an amorphous, interconnected pore network are likely to be conducive to the flow of oxygen and nutrients into and out of the bulk biomaterial scaffold, allowing them to act as viable support matrices for entrapped cells. Therefore, PNN-HA.RGDS, which has a high water content, open-pore network and adhesion peptides to support attachment of anchorage-dependent RPE cells, exhibits desirable characteristics to act as a synthetic cellular support matrix.

### *In vitro* cell viability

A culture of preadhered RPE cells was incubated with solutions of supplemented DMEM-F12 medium containing dissolved polymer samples PNN-10, PNN-HA, PNN-RGDS, and PNN-HA.RGDS. Culture medium containing no dissolved polymer was used as a control. RPE viability remained very high under all conditions following 96 h of exposure, Figure 6. There were no statistically significant differences among the mean RPE viabilities when cultured in the presence of the various copolymers ($p = 0.103$). These initial studies were intended to provide information about the compatibility of a model RPE cell line with the various copolymers. In future studies, we hope to examine scaffold compatibility with RPE derived from iPS cells. In these studies, we will examine the ability to differentiate iPS cells into RPE cells while cultured within PNN-RGDS and PNN-HA.RGDS scaffolds. Additionally, we will examine characteristics such as RPE polarity, the ability to phagocytose shed particles from photoreceptor outer segments and the efficiency of cellular entrapment and isolation within the biomaterial scaffold.

### Subcutaneous injections in SKH1-E mice

Although the intended application of these scaffolds is a minimally invasive delivery vehicle for posterior segment

**FIGURE 7.** SKH1-E mouse immediately following injection of PNN-10 into the subcutaneous space between the shoulder blades. The copolymer rapidly gelled into a mechanically robust lump following injection, indicated with the dashed line.

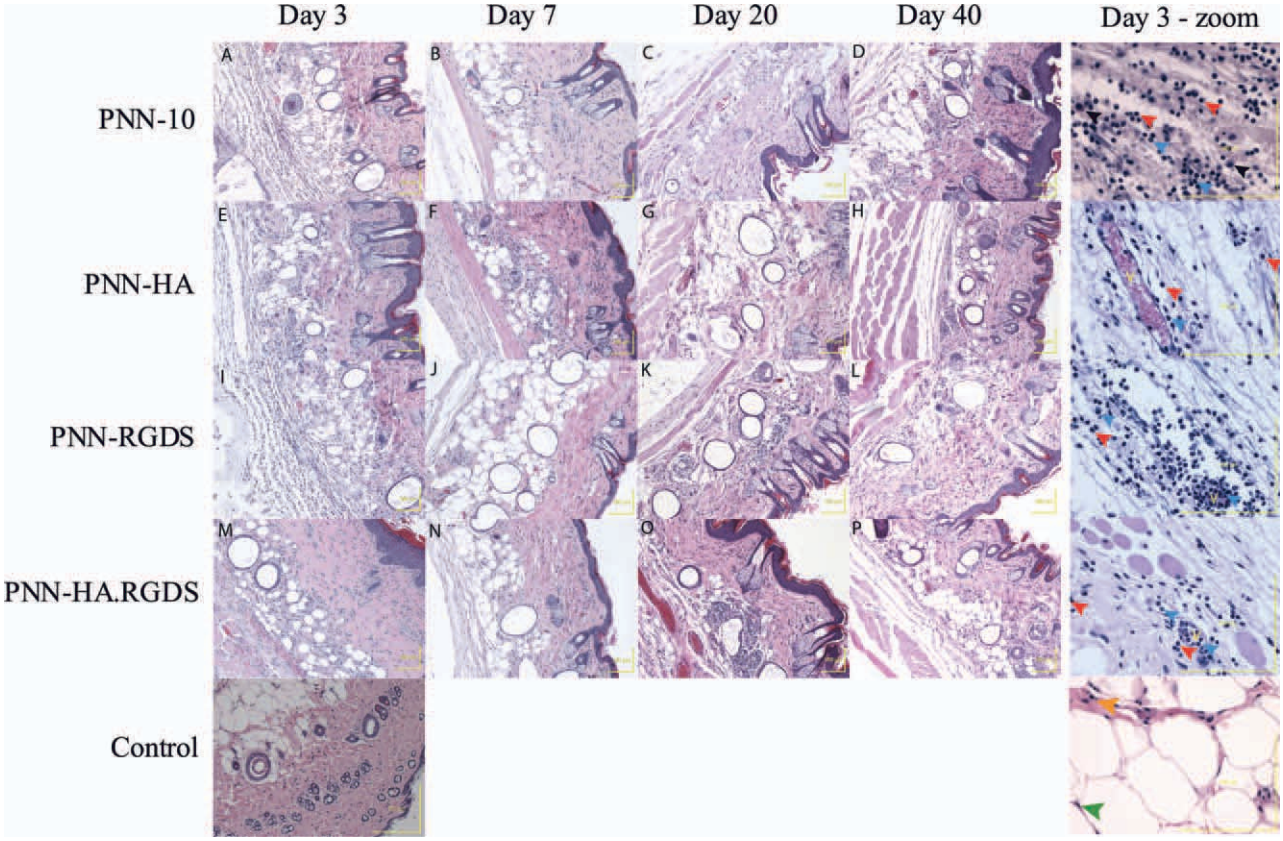


**FIGURE 8.** Histological sections of tissue at the injection site of PNN-10 (A–D), PNN-HA (E–H), PNN-RGDS (I–L), and PNN-HA.RGDS (M–P). From left to right, tissues were explanted on days 3, 7, 20, and 40 days postimplantation. Neutrophils, lymphocytes, monocytes, fibroblastic cells, and adipose cells are labeled with blue, red, black, orange and green arrows respectively in the magnified images from day samples (R–V). Scale bar = 100 μm. [Color figure can be viewed in the online issue, which is available at wileyonlinelibrary.com.]

therapeutics, in accordance with the McMaster University Animal Research Ethics Board, we were required to demonstrate material safety prior to intraocular injections. Therefore, our initial *in vivo* studies examine the host response to subcutaneous injections of copolymer suspensions between the shoulder blades of nude SKH1-E mice. All samples formed an observable, mechanically robust gel immediately upon injection into the subcutaneous space, Figure 7.

In all samples except for PNN-10 (day 3), the gelled material spread out into an apparent thin layer beneath the skin. This scaffold thinning provides favorable conditions for delivery of therapeutic cells into the subretinal space. Initial gel formation may prevent efflux of the cells and scaffold into the vitreous chamber and subsequent material spreading will promote migration within the subretinal space, maximizing coverage of the transplanted cells allowing a

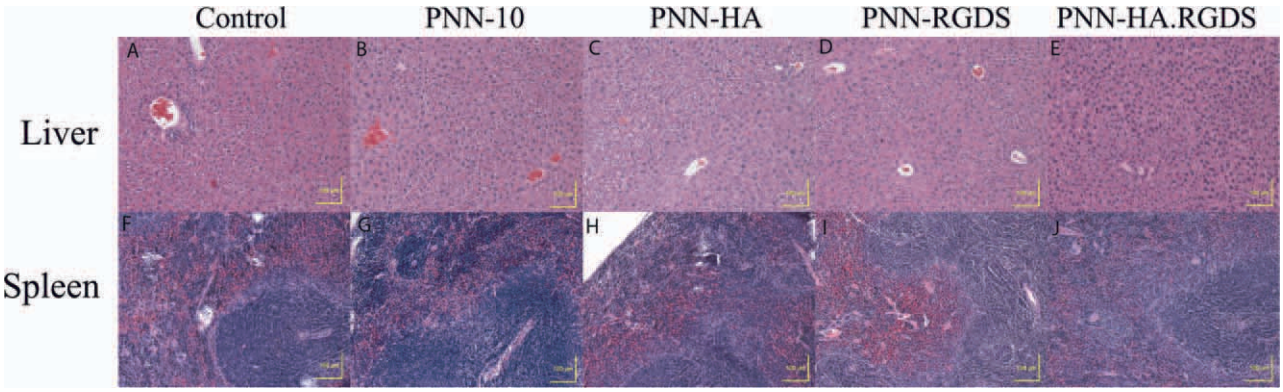


**FIGURE 9.** The top column shows H&E stained liver sections obtained from mice after 40 days of exposure to control (a), PNN-10 (b), PNN-HA (c), PNN-RGDS (d), and PNN-HA.RGDS (e). The second column (f–j) contains spleen sections in the same conformation. Scale bar =100 μm. [Color figure can be viewed in the online issue, which is available at wileyonlinelibrary.com.]

single injection to treat a relatively large area.[14] Furthermore, material thinning will minimize visual distortions, which may be caused by protrusion of the gelled scaffold behind the retina. However, the material spreading process made histological analysis of the tissues surrounding the implanted polymer challenging, as it was difficult to locate and identify discrete polymer regions. Therefore, histological sections were obtained by excising tissue from the initial injection site, Figure 8.

Mice were sacrificed at days 3, 7, 20, and 40 postinjection ($n$ = 1, 3, 2, and 2, respectively). Histology revealed a relatively minor response to the injected copolymers at day 3. There was an infiltration of immune cells where dermal tissue had been disturbed by the injection. The presence of darkly stained nuclei of leukocytes and fibroblasts indicate a mild inflammatory response consistent with the early stages of the foreign body reaction (FBR). There was no evidence of epidermal necrosis or basophilic debris to indicate acute cytotoxicity in either the dermis or epidermis. At this early stage in the foreign body response, neutrophils predominantly characterize the response (blue arrows). However, there was evidence of progression, with lymphocytes (red arrow) and monocytes (black arrow) infiltrating the implantation site. The infiltration of these leukocytes is often observed perivascularly (blood vessels are denoted with a "V"), indicating chemotaxis from the blood. The control sample shows no evidence of infiltrating cells within the dermis. Fibroblastic cells were labeled with an orange arrow and adipose cells with a green arrow. By day 7, all samples receiving injections appear to have returned to their native state, with no apparent signs of adverse reactivity for the duration of the 40-day experimental period. There was no evidence of fibroplasia or granuloma formation, and there was no histological evidence to suggest infection or hypersensitization.

Because histological sections of tissues surrounding defined polymer films were difficult to obtain, the liver and spleen were removed and sectioned after 40 days of implant exposure, Figure 9. The liver is responsible for metabolising and eliminating foreign materials and contains specialized resident macrophages, termed Kupffer cells, as well as deposited blood born macrophages. If nonstaining copolymers are phagocytosed by these cells, polymer accumulation in the liver will appear as vacuolated cells within the sinusoids of the liver. The spleen is another bioaccumulatory site, which metabolises some metabolites that bypass the liver. Detrimental polymer-induced effects may show up as abnormalities in these tissues.

There was no evidence of necrosis or inflammation of the liver from any of these samples. The anatomy captured in all four samples, Figure 9(b–e), show no marked differences from the control mouse, which received no injection. Furthermore, there was no evidence of accumulated phagocytic cells containing polymer that had escaped the site of injection. The masses of the livers (nondessicated) when removed from the mice were (A) = 1.48 g, (B) = 1.44 g, (C) = 1.51 g, (D) = 1.50 g, and (E) = 1.39 g. There was no evidence of liver hypertrophy, neoplastic proliferation, or necrosis. In the spleen, both the red and white pulp were free of visible vacuolated cells from the mononuclear phagocyte system. Furthermore, there was no evidence of splenomegaly or necrosis in any of the samples. None of the examined organs demonstrated any morphological abnormalities, and were indistinguishable from the control sample. The masses of the spleens (nondessicated) when removed from the mice were (F) = 85 mg, (G) = 90 mg, (H) =78 mg, (I) = 84 mg, and (J) = 88 mg.

Histological analysis of tissue at the injection site as well as the liver and spleen were not indicative of any adverse host reaction to the presence of the various p(NIPAAm-*co*-NAS)-based copolymers and warrant further studies in an intraocular setting.

## CONCLUSION

Copolymers of NIPAAm and NAS were synthesized via free radical polymerization and conjugated with amine-functionalized hyaluronic acid and cell adhesive RGDS peptides. These novel copolymers were designed to provide noninvasive delivery of therapeutic cells into the hard-to-access subretinal space for the treatment of retinal degenerative diseases, such as AMD and diabetic retinopathy. A subphysiological phase transition was conserved by incorporating a 90 mol % NIPAAm content into the copolymers. An LCST that is below body temperature allows the delivery of a liquid suspension of cells at room temperature that undergoes a rapid, thermally induced phase transition as the polymer is heated, forming a cell-infused scaffold *in situ*. Ultimately, this strategy is designed to increase the efficiency of subretinal cell delivery, while decreasing invasiveness of the procedure and providing anchorage-dependant RPE cells with a scaffold to act as an adhesion substrate. It may also be possible to load the liquid polymer/cell suspension with pharmaceuticals, growth factors or guidance molecules, creating a hybrid drug releasing cell scaffold capable of manipulating the conditions within the injection microenvironment. For example, corticosteroids may be coadministered to shore-up complications of macular edema,[43] or anti-VEGF agents could be employed to combat ocular neovascularization.[44] These scaffolds demonstrated excellent compatibility with RPE cells *in vitro* and histological analysis following subcutaneous injection between the shoulder blades of SKH1-E mice revealed a mild inflammatory response at day 3 that subsided by day 7. Future studies will examine copolymer drug release profiles, the ability to differentiate and sustain RPE cells from iPS cells, histological analysis of ocular tissues following injection of the scaffold into the vitreous and subretinal space and the development of a degradable PNIPAAm backbone that ultimately allows the complete clearance of the synthetic scaffold from the body.

## REFERENCES


1. Takahashi K, Yamanaka S. Induction of pluripotent stem cells from mouse embryonic and adult fibroblast cultures by defined factors. Cell 2006;126:663–676.
2. Marchetti V, Krohne TU, Friedlander DF, Friedlander M. Stemming vision loss with stem cells. J Clin Invest 2010;120:3012–3021.

3. MacLaren RE, Pearson RA, MacNeil A, Douglas RH, Salt TE, Akimoto M, Swaroop A, Sowden JC, Ali RR. Retinal repair by transplantation of photoreceptor precursors. Nature 2006;444:203–207.
4. West EL, Pearson RA, Tschernutter M, Sowden JC, MacLaren RE, Ali RR. Pharmacological disruption of the outer limiting membrane leads to increased retinal integration of transplanted photoreceptor precursors. Exp Eye Res 2008;86:601–611.
5. Eiraku M, Takata N, Ishibashi H, Kawada M, Sakakura E, Okuda S, Sekiguchi K, Adachi T, Sasai Y. Self-organizing optic-cup morphogenesis in three-dimensional culture. Nature 2011;472:51–56.
6. Marc RE, Jones BW, Watt CB, Strettoi E. Neural remodeling in retinal degeneration. Prog Retin Eye Res 2003;22:607–655.
7. West EL, Pearson RA, MacLaren RE, Sowden JC, Ali RR. Cell transplantation strategies for retinal repair. Prog Brain Res 2009;175:3–21.
8. Ming M, Li X, Fan X, Yang D, Li L, Chen S, Gu Q, Le W. Retinal pigment epithelial cells secrete neurotrophic factors and synthesize dopamine: Possible contribution to therapeutic effects of RPE cell transplantation in Parkinson's disease. J Transl Med 2009;7:53.
9. Zayit-Soudry S, Moroz I, Loewenstein A. Retinal pigment epithelial detachment. Survey Ophthalmol 2007;52:227–243.
10. Gouras P, Flood MT, Kjedbye H, Bilek MK, Eggers H. Transplantation of cultured human retinal epithelium to Bruch's membrane of the owl monkey's eye. Curr Eye Res 1985;4:253–265.
11. Lane C, Boulton M, Marshall J. Transplantation of retinal pigment epithelium using a pars plana approach. Eye (Lond) 1989;3(Part 1): 27–32.
12. da Cruz L, Chen FK, Ahmado A, Greenwood J, Coffey P. RPE transplantation and its role in retinal disease. Prog Retin Eye Res 2007;26:598–635.
13. Mooney DJ, Vandenburgh H. Cell delivery mechanisms for tissue repair. Cell Stem Cell 2008;2:205–213.
14. Ballios BG, Cooke MJ, van der Kooy D, Shoichet MS. A hydrogel-based stem cell delivery system to treat retinal degenerative diseases. Biomaterials 2009;31:2555–2564.
15. Gullapalli VK, Sugino IK, Van Patten Y, Shah S, Zarbin MA. Impaired RPE survival on aged submacular human Bruch's membrane. Exp Eye Res 2005;80:235–248.
16. Tezel TH, Del Priore LV, Kaplan HJ. Reengineering of aged Bruch's membrane to enhance retinal pigment epithelium repopulation. Investigative Ophthalmol Vis Sci 2004;45:3337–3348.
17. Del Priore LV, Geng L, Tezel TH, Kaplan HJ. Extracellular matrix ligands promote RPE attachment to inner Bruch's membrane. Current Eye Res 2002;25:79–89.
18. Fitzpatrick SD, Mazumder MAJ, Lasowski F, Fitzpatrick LE, Sheardown H. PNIPAAm-grafted-collagen as an injectable, in situ gelling, bioactive cell delivery scaffold. Biomacromolecules 2010;11: 2261–2267.
19. Tezel TH, DelPriore LV. Reattachment to a substrate prevents apoptosis of human retinal pigment epithelium. Graefes Arch Clin Exp Ophthalmol 1997;235:41–47.
20. Khademhosseini A, Eng G, Yeh J, Fukuda J, Blumling J, Langer R, Burdick JA. Micromolding of photocrosslinkable hyaluronic acid for cell encapsulation and entrapment. J Biomed Mater Res Part A 2006;79:522–532.
21. Kim J, Park Y, Tae G, Lee KB, Hwang CM, Hwang SJ, Kim IS, Noh I, Sun K. Characterization of low-molecular-weight hyaluronic acid-based hydrogel and differential stem cell responses in the hydrogel microenvironments. J Biomed Mater Res Part A 2009;8:967–975.
22. Zeng F, Tong Z, Sato T. Molecular chain properties of poly( N-isopropyl acrylamide). Sci China Series B-Chem 1999;42:290–297.
23. Holy CE, Cheng C, Davies JE, Shoichet MS. Optimizing the sterilization of PLGA scaffolds for use in tissue engineering. Biomaterials 2001;22:25–31.
24. Guan J, Hong Y, Ma Z, Wagner WR. Protein-reactive, thermoresponsive copolymers with high flexibility and biodegradability. Biomacromolecules 2008;9:1283–1292.
25. Oliviero G, Bergese P, Canavese G, Chiari M, Colombi P, Cretich M, Damin F, Fiorilli S, Marasso SL, Ricciardi C, Rivoloc P, Deperoa LE. A biofunctional polymeric coating for microcantilever molecular recognition. Anal Chim Acta 2008;630:161–167.
26. Xu J, Tao L, Boyer C, Lowe AB, Davis TP. Facile access to polymeric vesicular nanostructures: Remarkable ω-end group effects in cholesterol and pyrene functional (Co)polymers. Macromolecules 2011;44:299–312.
27. Thomson HA, Treharne AJ, Backholer LS, Cuda F, Grossel MC, Lotery AJ. Biodegradable poly(alpha-hydroxy ester) blended microspheres as suitable carriers for retinal pigment epithelium cell transplantation. J Biomed Mater Res Part A 2010;95: 1233–1243.
28. Laurent TC, Fraser JRE. Hyaluronan. FASEB J 1992;6:2397–2404.
29. Gutowska A, Jeong B, Jasionowski M. Injectable gels for tissue engineering. Anatomical Record 2001;263:342–349.
30. Limberg MB, McCaa C, Kissling GE, Kaufman HE. Topical application of hyaluronic-acid and chondroitin sulfate in the treatment of dry eyes. Am J Ophthalmol 1987;103:194–197.
31. Aragona P, Papa V, Micali A, Santocono M, Milazzo G. Long term treatment with sodium hyaluronate-containing artificial tears reduces ocular surface damage in patients with dry eye. Br J Ophthalmol 2002;86:181–184.
32. Nishida T, Nakamura M, Mishima H, Otori T. Hyaluronan stimulates corneal epithelial migration. Exp Eye Res 1991;53:753–758.
33. Goa KL, Benfield P. Hyaluronic acid—A review of its pharmacology and use as a surgical aid in ophthalmology, and its therapeutic potential in joint disease and wound-healing. Drugs 1994;47: 536–566.
34. Van Beek M, Jones L, Sheardown H. Hyaluronic acid containing hydrogels for the reduction of protein adsorption. Biomaterials 2008;29:780–789.
35. Uludag H, Norrie B, Kousinioris N, Gao TJ. Engineering temperature-sensitive poly(N-isopropylacrylamide) polymers as carriers of therapeutic proteins. Biotechnol Bioeng 2001;73:510–521.
36. Ohya S, Sonoda H, Nakayama Y, Matsuda T. The potential of poly(N-isopropylacrylamide) (PNIPAM)-grafted hyaluronan and PNIPAM-grafted gelatin in the control of post-surgical tissue adhesions. Biomaterials 2005;26:655–659.
37. Tan H, Ramirez CM, Miljkovic N, Li H, Rubin JP, Marra KG. Thermosensitive injectable hyaluronic acid hydrogel for adipose tissue engineering. Biomaterials 2009;30:6844–6853.
38. Smith E, Bai J, Oxenford C, Yang J, Somayaji R, Uludag H. Conjugation of arginine-glycine-aspartic acid peptides to thermoreversible N-isopropylacrylamide polymers. J Polym Sci Part A: Polym Chem 2003;41:3989–4000.
39. Smith E, Yang J, McGann L, Sebald W, Uludag H. RGD-grafted thermoreversible polymers to facilitate attachment of BMP-2 responsive C2C12 cells. Biomaterials 2005;26:7329–7338.
40. Li F, Griffith M, Li Z, Tanodekaew S, Sheardown H, Hakim M, Carlsson DJ. Recruitment of multiple cell lines by collagen-synthetic copolymer matrices in corneal regeneration. Biomaterials 2005;26:3093–3104.
41. Quan C-Y, Chen J-X, Wang H-Y, Li C, Chang C, Zhang X-Z, Zhuo R-X. Core-shell nanosized assemblies mediated by the alpha-beta cyclodextrin dimer with a tumor-triggered targeting property. ACS Nano 2010;4:4211–4219.
42. Cui ZW, Lee BH, Vernon BL. New hydrolysis-dependent thermosensitive polymer for an injectable degradable system. Biomacromolecules 2007;8:1280–1286.
43. Edelman JL, Lutz D, Castro MR. Corticosteroids inhibit VEGF-induced vascular leakage in a rabbit model of blood-retinal and blood-aqueous barrier breakdown. Exp Eye Res 2005;80: 249–258.
44. Jardeleza MS, Miller JW. Review of anti-VEGF therapy in proliferative diabetic retinopathy. Semin Ophthalmol 2009;24:87–92.